Inorganic Chemistry

Article

pubs.acs.org/IC

Quaternary Aluminum Silicides Grown in Al Flux: $RE_5Mn_4Al_{23-x}Si_x$ (RE = Ho, Er, Yb) and $Er_{44}Mn_{55}(AlSi)_{237}$

Nicholas P. Calta[†] and Mercouri G. Kanatzidis*[,†,‡]

[†]Department of Chemistry, Northwestern University, Evanston, Illinois 60208, United States

[‡]Materials Science Division, Argonne National Laboratory, Argonne, Illinois 60439, United States

S Supporting Information

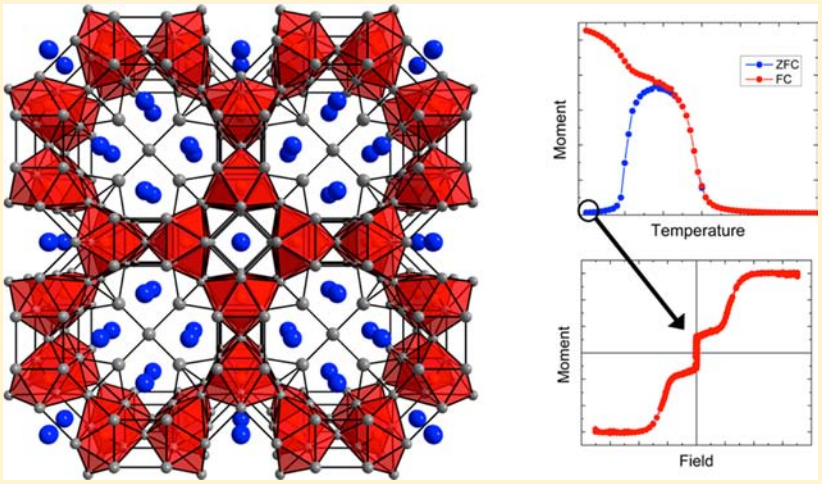

ABSTRACT: Four novel intermetallic silicides, $RE_5Mn_4Al_{23-x}Si_x$ (x = 7.9(9), RE = Ho, Er, Yb) and $Er_{44}Mn_{55}(AlSi)_{237}$, have been prepared by reaction in aluminum flux. Three $RE_5Mn_4Al_{23-x}Si_x$ compounds crystallize in the tetragonal space group $P4/mmm$ with the relatively rare $Gd_5Mg_5Fe_4Al_{18-x}Si_x$ structure type. Refinement of single-crystal X-ray diffraction data yielded unit cell parameters of a = 11.3834(9)−11.4171(10) Å and c = 4.0297(2)−4.0575(4) Å with volumes ranging from 522.41(5) to 528.90(8) Å^3. Structure refinements on single-crystal diffraction data show that $Er_{44}Mn_{55}(AlSi)_{237}$ adopts a new cubic structure type in the space group $Pm\bar{3}n$ with a very large unit cell edge of a = 21.815(3) Å. This new structure is best understood when viewed as two sets of nested polyhedra centered on a main group atom and a manganese atom. These polyhedral clusters describe the majority of the atomic positions in the structure and form a perovskite-type network. We also report the electrical and magnetic properties of the title compounds. All compounds except the Ho analogue behave as normal paramagnetic metals without any observed magnetic transitions above 5 K and exhibit antiferromagnetic correlations deduced from the value of their Curie constants. $Ho_5Mn_4Al_{23-x}Si_x$ exhibits a ferromagnetic transition at 20 K and an additional metamagnetic transition at 10 K, suggesting independent ordering temperatures for two distinct magnetic sublattices.

■ INTRODUCTION

Rare earth-containing intermetallic compounds exhibit a wide variety of interesting structural and physical properties including heavy fermion behavior,[1−4] superconductivity,[5−7] Kondo physics,[8−10] quantum criticality,[11−13] and interesting magnetic ordering.[14−17] While this diversity of properties is fascinating, prediction of these behaviors remains elusive. Therefore, the availability of new phases via discovery synthesis and their subsequent characterization is of particular importance to intermetallic chemistry, as new compounds can validate existing insights or generate new ones. In recent years, we have explored a number of RE/T/Al/Si systems, where RE is a rare earth element and T is a transition metal, using aluminum flux as a reaction medium.[18−24] Flux reactions provide many synthetic advantages, including increased diffusion of reactants to improve reactivity and single-crystal growth.[25−27] These reactions also allow for lower reaction temperature than traditional solid-state techniques or arc melting, providing a route to access kinetically stabilized phases that do not otherwise appear in the phase diagram.

Aluminum flux reactions have yielded rare earth transition metal aluminum silicides and germanides with a wide variety of properties. $REFe_4Al_9Si_6$ (RE = Tb, Er) exhibits exceptionally robust oxidation resistance at high temperature by forming a passivating surface layer of oxide, gaining less than 1% by mass upon heating in air to 900 °C.[24] Many compounds in this class magnetically order in some way at low temperature, on the

Received: May 3, 2013
Published: August 9, 2013

order of 50 K or below. The most magnetically interesting members include the germanide $SmNiAl_4Ge_2$, which displays complex magnetic behavior partially consistent with geometric spin frustration.[19] Similarly, $Dy_2MAl_6Si_4$ (M = Au, Pt) both show antiferromagnetic ordering transitions at around 10 K and metamagnetic behavior in field-dependent studies at 3 K. This has been tentatively attributed to a two-step spin reorientation at higher fields, with ferromagnetic ordering of inequivalent Dy sites dominating at higher fields.[23] Additionally, Yb-containing intermetallics often exhibit interesting effects as a result of mixed or other unusual valence effects due to the stability of both Yb^{2+} and Yb^{3+}, as observed in $YbAu_{3.86}Al_8Si_{1.14}$[28] and $Yb_3Au_{6+x}Al_{26}Ti$.[29]

Rare earth transition metal aluminum silicides exhibit a diversity of structural features in addition to physical properties. $Gd_{2x/3}Pt_{1+x}(Al,Si)_{3x+2}$ (x = 1, 2) exhibits a disordered Gd/Al layer intergrown between Al- and Pt-containing layers.[30] The homologous series $RE(AuAl_2)_nAl_2(Au_xSi_{1-x})_2$ (n = 3, x = ~0.5) also exhibits a layered intergrowth, with slabs of the $BaAl_4$ structure and antifluorite-type layers of $AuAl_2$,[28,31] as does $RE_2MAl_6Si_4$ (RE = Gd, Tb, Dy; M = Au, Pt) with alternating $CaAl_2Si_2$- and $YNiAl_4Ge_2$-type slabs with monatomic rare earth layers intervening between the more complex layers.[23] This class of compounds not only adopts layered structures, however; $RE_8Ru_{12}Al_{49}Si_9(Al_xSi_{12-x})$ (RE = Pr or Sm) forms a complex three-dimensional cubic structure based on a variety of interconnected clusters.[20] In addition to the structural features of these sorts of related rare earth compounds, the introduction of Mn into the aluminum silicide system increases the likelihood of quasicrystal formation.[32] The Mn—Al—Si ternary system contains rather extensively studied quasicrystals[33] and their approximant phases.[34]

We chose the RE/Mn/Al/Si system as an extension of the RE/Fe/Al/Si system to see if Mn analogues of either $REFe_4Al_9Si_6$ or $RE_4Fe_{2+x}Al_{7-x}Si_8$ exist. There is only a single report of a compound with a RE/Mn/Al/Si composition,[35] $GdAl_{2-x}Mn_xSi_2$. It is a layered compound that exhibits positionally disordered Mn atoms and is structurally very different from the quaternary Fe-containing phases discussed above. While no evidence for analogues of the iron compounds was found, four new intermetallic compounds were discovered via reaction in Al flux: $RE_5Mn_4Al_{23-x}Si_x$ (x = 7.9(9), RE = Ho, Er, Yb) and $Er_{44}Mn_{55}(AlSi)_{237}$. All crystallize in either rare or unreported structure types. We report the synthesis, structure, magnetic, and electrical properties of all four compounds.

EXPERIMENTAL DETAILS

General Experimental Details. All manipulations involving air-sensitive rare earth elements and Mn were carried out in a nitrogen glovebox. All materials were used as purchased without further purification. Reactions used Ho, Er, and Yb powder (hand-ground from ingot, Atlantic Equipment Engineers), Mn powder (99%, 325 mesh, Aldrich), Si powder (99.96%, 325 mesh, Cerac), and Al shots (99.8%, Alfa Aesar). NaOH (EMD, pellets, 99%) was used in purification.

Synthesis of $RE_5Mn_4Al_{23-x}Si_x$ (RE = Er, Ho, Yb). Al (30 equiv) and Si (10 equiv) were added to alumina crucibles on a 0.5 mmol (~1 g total) scale, which were then transferred into a glovebox. In the box, Mn (4 equiv) and rare earth element (5 equiv) were also added to the crucibles. The crucibles were removed from the box and sealed in jacketing silica tubes evacuated to 10^{-4} mbar. The reactions were placed in a tube furnace and heated to 960 °C in 12 h, held at that temperature for 4 days, and cooled to room temperature in 10 h. Quenching the reaction rather then furnace-cooling it also yields the target compound. The resulting ingot was etched in <5 M NaOH to remove excess Al flux. In the Er-containing reactions, this yielded a mixture of products, primarily $Mn_2Al_{8.36}Si_{1.14}$, ErAlSi, and $Er_3Al_2Si_2$, along with a few rod-shaped crystals of $Er_5Mn_4Al_{23-x}Si_x$, in some cases as large as ~500 μm long. The total yield of the target compound in these reactions was <10%, as estimated from powder diffraction patterns. A few smaller crystals of $Er_{44}Mn_{55}(AlSi)_{237}$ were observed as well. In the Ho- and Yb-containing reactions, the reactions yielded a less diverse mixture, with the target compound and unreacted Al flux the two most prominent phases observed by powder X-ray diffraction. Yields of the Ho and Yb reactions, as estimated from relative intensity of peaks in powder diffraction patterns, were roughly 80% and 70%, respectively. Many efforts to synthesize Tm and Y analogues failed, despite their similarity to Er, Ho, and Yb in atomic radius.

Synthesis of $Er_{44}Mn_{55}(AlSi)_{237}$. Al (20 equiv) and Si (6 equiv) were added to alumina crucibles on a 0.4 mmol scale (~0.8 g total), which were then transferred into a glovebox. In the box, Mn (2 equiv) and Er (2 equiv) were also added to the mixture, and then sealed in silica tubes evacuated to 10^{-4} mbar. The reactions were then placed in a tube furnace and heated to 850 °C in 12 h, held at that temperature for 7 days, then cooled to 500 °C in 2 days, and finally cooled to room temperature in 12 h. The resulting ingot was etched in NaOH to remove excess Al flux, and yielded a mixture of products. The most common phases were $Er_3Al_2Si_2$ $Mn_2Al_{8.36}Si_{1.14}$, and some small crystals of $Er_{44}Mn_{55}(AlSi)_{237}$, which had to be mechanically isolated. These reactions also yielded a few small crystals of $Er_5Mn_4Al_{23-x}Si_x$. The title compounds in these reactions are hardly observable by powder diffraction, so estimation of exact yield proved difficult.

Single-Crystal X-ray Diffraction. Single-crystal diffraction measurements were carried using both a STOE2T and a STOE2 diffractometer controlled by the X-Area suite of programs.[36] All collections were carried out at room temperature using Mo Kα radiation (λ = 0.71073 Å). Many crystals from each reaction mixture were screened to obtain unit cell parameters. On the basis of screened frames, full spheres of diffraction data were collected on the best crystals. Analytical absorption corrections were applied using the program X-Red32 of the X-Area suite. The crystal structures were solved using direct methods and refined using the SHELX suite.[37] After refinement, atomic positions were standardized using StructureTidy in PLATON.[38,39] In the case of $Er_{44}Mn_{55}(AlSi)_{237}$, Al/Si positions were mixed in a 1:1 ratio based on elemental analysis results, as we could not distinguish between them due to the limits of X-ray diffraction. In the case of $RE_5Mn_4Al_{23-x}Si_x$, Al and Si positions were tentatively assigned based on bond length,[22,23] but upon further analysis of the structure we concluded that meaningful site assignments could not be made on the basis of bond length alone, and all of the main group sites were assigned with fixed mixed compositions based on elemental analysis results. Neutron diffraction studies are required to make conclusive site assignments.

Powder X-ray Diffraction. Phase identity and purity of reaction mixtures were checked on an Inel CPS120 in reflectance geometry using Cu Kα radiation (λ = 1.5406 Å). Samples were affixed to borosilicate slides using double-sided tape.

Scanning Electron Microscopy-Electron Dispersive X-ray Spectroscopy (SEM-EDS). Crystal images and approximate elemental compositions were determined using a Hitachi S3400N-II scanning electron microscope (SEM) with an Oxford Instruments INCAx-act SDD EDS detector. Known EDS samples used to standardize the instrument were elemental Mn, Al_2O_3, SiO_2, and ErF_3. Data were collected on unpolished single crystals mounted on carbon tape with an accelerating voltage of 20 kV and acquisition times of 60 s. Numerous clean surfaces of each crystal were analyzed to ensure uniformity. In a few instances, longer acquisition times of 300 s were used to obtain semiquantitative compositions.

Single-Crystal Resistivity Measurements. Four-point resistivity measurements were taken on large single crystals, whose identities were confirmed using both single-crystal X-ray diffraction and electron dispersive spectroscopy. Contacts were made by affixing copper wires to each crystal with colloidal silver paste. Measurements were taken using a Quantum Design PPMS between 2 and 300 K. Sample dimensions were determined by scanning electron microscopy.

Magnetic Properties Measurements. Magnetic measurements were taken using a Quantum Design MPMS-XL. Single-crystal samples were mounted on a quartz rod using glue. Measurements were taken with the applied field parallel to the *c*-axis or *a*-axis in the case of $Er_{55}Mn_{44}(AlSi)_{237}$. Sample mass was determined by geometrically measuring volume and computing mass based on theoretical density. Most measurements used one large single crystal, but some of the measurements taken on $Ho_5Mn_4Al_{23-x}Si_x$ used two single crystals aligned next to one another, glued inside a polycarbonate capsule wrapped in Teflon tape and contained in a straw.

RESULTS AND DISCUSSION

Synthesis. The reported compounds were originally synthesized in an effort to make Mn analogues of the previously observed iron-containing compounds $REFe_4Al_9Si_6$.[24] Aluminum flux was used as a reaction medium, as it provides a number of advantages for our synthetic target. It dissolves a large amount of silicon, leaving it in a reactive state. It also permits reactions at lower temperatures than conventional high temperature solid-state reactions without compromising reactant diffusion, providing an opportunity to synthesize kinetically stabilized phases. Finally, flux reactions often yield large single crystals, which are convenient for characterization. Because of the relatively rich chemistry of the RE/Mn/Al/Si system, synthetic efforts produce a number of undesired binary and ternary side products, resulting in low reaction yields. Er was the first rare earth element used and yielded two new compounds, $Er_5Mn_4Al_{23-x}Si_x$ and $Er_{44}Mn_{55}(AlSi)_{237}$. These two competing compounds seem to be very close to one another in energy; it proved nearly impossible to synthesize one without at least a few crystals of the other appearing in the product mixture. Interestingly, $Er_{55}Mn_{44}(AlSi)_{237}$ appears to be unique to the Er system, and no evidence of Ho or Yb analogues was seen. SEM images of representative crystals are shown in Figure 1.

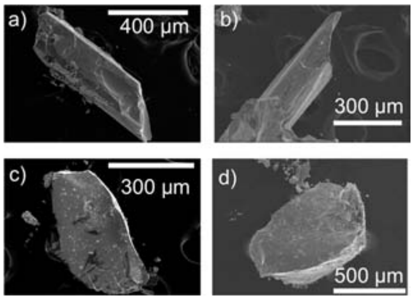

Figure 1. SEM images of typical crystals of the four title compounds. Images (a)−(c) depict $RE_5Mn_4Al_{23-x}Si_x$ (RE = Ho, Er, and Yb, respectively), and (d) depicts $Er_{44}Mn_{55}(AlSi)_{237}$.

Crystal Structure of $RE_5Mn_4Al_{23-x}Si_x$. Three of the four title compounds crystallize in the recently reported $Gd_5Mg_5Fe_4Al_xSi_{18-x}$ structure type[16] with the tetragonal space group *P*4/*mmm*, shown in Figure 2a. The unit cell parameters are $a = 11.3834(9)-11.4171(10)$ and $c = 4.0297(2)-4.0575(4)$ Å with volumes ranging from 522.41(5) to 528.90(8) Å^3, depending on the identity of the rare earth element (Table 1 and Figure 2b). They exhibit two unique rare earth positions, a single Mn position, and a three-dimensional framework of Al and Si atoms, listed in Table 2. The initial refinement assigned main group sites as either Al or Si based on a cursory look at bond length, which yielded an Al:Si ratio of 13:10. These tentative assignments were examined closely, as similar X-ray scattering factors of Al and Si prevent unambiguous assignment using X-ray data alone. EDS measurements on multiple different crystals yielded a composition of $RE_{4.7(1.1)}Mn_{3.9(9)}Al_{15.4(1.0)}Si_{8.1(1.1)}$, and after careful comparison of bond lengths in related Al- and Si-containing intermetallic compounds, we decided that the bond length segregation observed in $RE_5Mn_4Al_{23-x}Si_x$ is not sufficiently large to make conclusive site assignments. On the basis of the total number of main group atomic positions, Al and Si must add up to 23 at most. Freely refined occupancies and displacement parameters of main group positions suggested full occupancy on all sites. Using EDS data and the constraint that Al occupancy plus Si occupancy must total 23, each Al/Si site occupancy was fixed at an Al:Si ratio of 15.1:7.9 in the final refinement. The occupancy of each main group site was fixed at this ratio in the final refinement. No changes in overall *R* values were observed when making these site assignment changes for the main group elements, and displacement parameters of the atomic positions improved in some cases and became worse in others upon full mixing, causing no net difference. While we believe that site preferences for Al or Si do exist, neutron diffraction measurements are required to conclusively assign the occupancies of the main group sites.

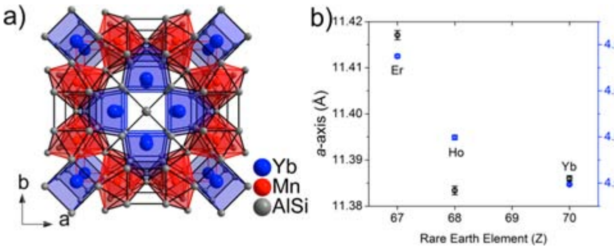

Figure 2. (a) Structure of $RE_5Mn_4Al_{23-x}Si_x$, with blue atoms representing RE element, red representing Mn, and gray representing mixed Al/Si sites. Coordination spheres around Mn and RE atoms are highlighted in red and blue, respectively. Unit cell parameters as a function of rare earth element are shown in (b).

Selected interatomic distances are listed in Table 3. In both cases, the rare earth atoms are located in channels along the *c*-axis and are separated by more than 4 Å, too far to be a genuine bonding interaction. The local environments of the rare earth positions differ in both geometry and the number of ligands that fill their coordination sphere. The RE1 atom on Wyckoff position 1*a* (Figure 3a) sits at the center of an elongated cube of Al/Si atoms, with uniform bond lengths varying between 2.8458(17) and 2.8587(13) Å, depending on the rare earth identity. This RE coordination resembles that of RE sites of the homologous series $RE(AuAl_2)_nAl_2(Au_xSi_{1-x})_2$, where Si atoms form compressed cubes around RE positions.[22] When stacked along the *c*-axis, these units form chains of an elongated CsCl-type motif. The RE2 atom (Figure 3b) is 9-coordinate and sits off-center in a monocapped, elongated cube of Al/Si atoms occupying the 4*k* and 8*q* positions. Three distinct bond lengths appear in this polyhedron: two with multiplicities of four that range from 2.8617(7)−2.8748(6) Å and 3.0269(13)−3.0495(11) Å, accounting for the eight ligands that form the elongated cube. One of the cube faces is capped with an additional main group atom sitting on the 4*f* position.

The Mn atom (Figure 3c) sits on the 4*l* position slightly offset from the middle of a triangular prism of main group

Table 1. Crystallographic Refinement Details for the Four Title Compounds

	empirical formula			
	$Ho_5Mn_4Al_{15.1}Si_{7.9}$	$Er_5Mn_4Al_{15.1}Si_{7.9}$	$Yb_5Mn_4Al_{15.1}Si_{7.9}$	$Er_{44}Mn_{55}(AlSi)_{237}$
formula wt	1673.70	1685.35	1714.27	33 814.98
temp (K)	293(2)	293(2)	293(2)	293(2)
wavelength (Å)	0.71073	0.71073	0.71073	0.71073
crystal system	tetragonal	tetragonal	tetragonal	cubic
space group	$P4/mmm$	$P4/mmm$	$P4/mmm$	$Pm\bar{3}n$
unit cell (Å)	a = 11.4171(10)	a = 11.3834(9)	a = 11.3860(6)	a = 21.8208(4)
	c = 4.0575(4)	c = 4.0399(5)	c = 4.0297(2)	
volume (Å^3)	528.90(8)	523.50(9)	522.41(5)	10 389.9(3)
Z	1			2
density (calcd)	5.262 g/cm^3	5.353 g/cm^3	5.449 g/m^3	5.404 g/cm^3
abs coefficient (mm^{-1})	21.868	23.239	25.552	21.960
F(000)	744	749	757	15 134
crystal size (μm)	114 × 50 × 79	41 × 34 × 7	60 × 50 × 11	20 × 20 × 40
θ range (deg)	1.78−29.11	1.79−29.15	1.79−29.18	1.32−25.00
index ranges	$-15 \le h \le 15$	$-13 \le h \le 15$	$-15 \le h \le 15$	$-25 \le h \le 25$
	$-15 \le k \le 15$	$-15 \le k \le 15$	$-15 \le k \le 15$	$-25 \le k \le 23$
	$-5 \le l \le 5$	$-5 \le l \le 5$	$-5 \le l \le 5$	$-25 \le l \le 25$
reflns collected	5141	5147	5163	56 227
indep reflns	468 [R_{int} = 0.0500]	470 [R_{int} = 0.0485]	469 [R_{int} = 0.0703]	1661 [R_{int} = 0.1166]
completeness	98.7%	100%	99.6%	99.9%
refinement	full-matrix least-squares on F^2	full-matrix least-squares on F^2	full-matrix least-squares on F^2	full-matrix least-squares on F^2
data/restraints/parameters	468/0/36	470/0/35	469/0/35	1661/0/149
GOF	1.386	1.374	1.196	1.445
final R indices [$>2\sigma(I)$]^a	R_{obs} = 0.0185	R_{obs} = 0.0263	R_{obs} = 0.0269	R_{obs} = 0.0502
	wR_{obs} = 0.0510	wR_{obs} = 0.0421	wR_{obs} = 0.0423	wR_{obs} = 0.0712
R indices [all data]	R_{all} = 0.0187	R_{all} = 0.0303	R_{all} = 0.0316	R_{all} = 0.0603
	wR_{all} = 0.0511	wR_{all} = 0.0428	wR_{all} = 0.0435	wR_{all} = 0.0730
extinction coeff	0.0096(7)	0.0026(2)	0.0023(2)	0.000014(3)
largest diff peak, hole (e Å^{-3})	0.945, −1.319	1.240, −1.874	1.630, −1.574	1.312, −1.712

$^aR = \sum||F_o| - |F_c||/\sum|F_o|$, $wR = [\sum[w(|F_o|^2 - |F_c|^2)^2]/\sum[w(|F_o|^4)]]^{1/2}$, and calcd $w = 1/[\sigma^2(F_o^2) + (0.0351P)^2 + 8.2030P]$ where $P = (F_o^2 + 2F_c^2)/3$.

ligands. This prism has each vertical face capped with additional Al/Si atoms whose bonding contacts to the Mn are actually shorter than those atoms in the prism. The triangular prisms share faces along the c-axis and capping ligands bridge the polyhedra in the ab plane. This arrangement yields a three-dimensional network of Mn-centered capped triangular prisms arranged in columns along the c-axis, which are connected through the capping Al/Si atoms that bridge the columns.

The above description of the $RE_5Mn_4Al_{23-x}Si_x$ structure solely in terms of polyhedra around the metal centers leaves out a single main group atom, situated at Wyckoff position 1d. It is 4-coordinate in a square planar arrangement, linking the distorted, capped cubes around the 9-coordinate rare earth position.

This structure type has been reported once before, by Ma and co-workers.[16] The most substantial difference between their report and the present one is the presence of Mg in the structure. The Mg atom exclusively occupies the 4j site, which in $RE_5Mn_4Al_{23-x}Si_x$ is a mixed Al/Si site. In these structures, the 4j site bridges two transition metal sites. This change in bridging atom identity could have a significant impact on magnetic ordering of the transition metal, but in both compounds the only moment arises from the rare earth elements, as discussed below, so it is unlikely that a change in bridging atom between Mn atoms directly affects magnetic behavior. In addition to this difference in bond topology, the Al/Si for Mg replacement also impacts the electron count per unit cell. The replacement of Mg by Al/Si electronically compensates for the change in transition metal from Fe to Mn. As a consequence, the electron count for both of these compounds is identical within the uncertainty range in x in $RE_5Mn_4Al_{23-x}Si_x$.

Crystal Structure of $Er_{44}Mn_{55}(AlSi)_{237}$. The fourth title compound crystallizes in a new structure type with the cubic space group $Pm\bar{3}n$ shown in Figure 4, with refinement details listed in Table 1. The unit cell edge length is 21.815(3) Å, yielding a large unit cell volume of 10382(2) Å^3, requiring 672 atoms to fill it, including 4 unique Er positions, 5 unique Mn positions, and 16 unique main group positions listed in Table 4, with selected interatomic distances in Table 5. As mentioned previously, X-ray diffraction cannot distinguish Al and Si atoms due to their similar scattering factors. In this cubic structure, tentative assignment by bond length proved impossible, so the assignments during refinement were made arbitrarily. To determine Al/Si content, elemental analysis data were necessary. A number of EDS measurements were taken, resulting in an average composition of $Er_{52(9)}Mn_{62(11)}Al_{113(9)}Si_{107(12)}$. These values are in agreement with the composition obtained from diffraction of $Er_{44}Mn_{55}(AlSi)_{237}$. We assumed full occupancy for all main group sites so as to allow the refinement to converge satisfactorily, suggesting an Al stoichiometry of 122(16) and a corresponding Si stoichiometry of 115(16), or an Al:Si ratio of 51(6):49(6). In the final refinement, the main group site occupancies were mixed in a fixed 1:1 Al:Si ratio based on these EDS results. We will refer to the Al/Si sites as X to simplify the

Table 2. Atomic Positions for $RE_5Mn_4Al_{23-x}Si_x$ Compounds[a]

atom	x	y	z	Wyckoff label	U_{eq}
Ho(1)	0	0	0	1a	7(1)
Er(1)	0	0	0		6(1)
Yb(1)	0	0	0		5(1)
Ho(2)	1/2	0.2672(1)	0	4n	6(1)
Er(2)	1/2	0.2674(1)	0		5(1)
Yb(2)	1/2	0.2674(2)	0		6(1)
Mn(1)	0	0.2915(2)	0	4l	5(1)
	0	0.2921(2)	0		4(1)
	0	0.2917(2)	0		5(1)
Al/Si(1)	0.2013(2)	0.2013(2)	0	4j	12(1)
	0.2011(2)	0.2011(2)	0		10(1)
	0.2051(2)	0.2051(2)	0		10(1)
Al/Si(2)	0.3689(2)	0.1169(2)	1/2	8q	8(1)
	0.3692(2)	0.1172(2)	1/2		8(1)
	0.3701(2)	0.1175(2)	1/2		8(1)
Al/Si(3)	1/2	1/2	1/2	1d	9(1)
	1/2	1/2	1/2		10(2)
	1/2	1/2	1/2		11(2)
Al/Si(4)	0.1764(2)	0	1/2	4m	4(1)
	0.1761(2)	0	1/2		4(1)
	0.1778(2)	0	1/2		4(1)
Al/Si(5)	0.3350(2)	0.3350(2)	1/2	4k	3(1)
	0.3354(2)	0.3354(2)	1/2		3(1)
	0.3345(2)	0.3345(2)	1/2		3(1)
Al/Si(6)	0	1/2	0	2f	6(1)
	0	1/2	0		6(1)
	0	1/2	0		5(1)

[a] For each atomic position, the first row refers to the Ho analogue, followed by Er and then Yb. U_{eq} is defined as one third of the trace of the orthogonalized U_{ij} tensor with units $Å^2 \times 10^{-3}$.

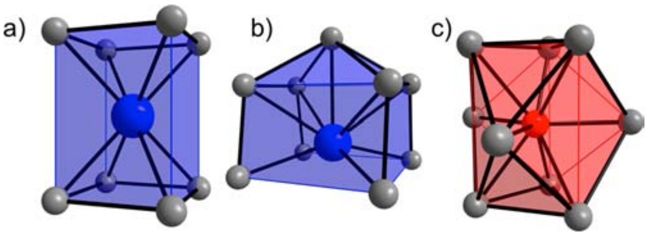

Figure 3. Individual atomic environments in $RE_5Mn_4Al_{23-x}Si_x$, including (a) the distorted main group cube around RE1 position, (b) the 9-ligand coordination environment of the RE2 position, and (c) the capped trigonal prism around the Mn position.

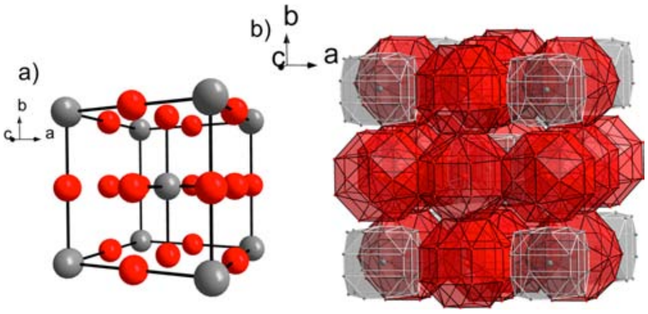

Figure 4. Schematic representation of the perovskite-type network in $Er_{44}Mn_{55}(AlSi)_{237}$ made up of the lattice of nested polyhedra centered on Mn5 (red) and X16 (gray). In (a) the polyhedra are simplified into spheres, and in (b) they are shown fully. All "bonds" shown in (a) consist of direct Mn—main group atom bonds between the outer shells of the two sets of nested polyhedra. The nested polyhedra themselves are shown in more detail in Figures 5 and 6.

discussion. Because of its high complexity, the structure is best understood when viewed as a series of nested polyhedra centered on Mn5 (Figure 5) and X16 (Figure 6).

Mn5 occupies Wyckoff position 6*b*, and is surrounded by six main-group atoms arranged in a Jahn—Teller distorted octahedron with two short bond lengths of 2.441(6) Å and four long bond lengths of 2.515(4) Å. The faces of this octahedron are each capped by an Er atom, which form a slightly distorted cube centered on the Mn5 site, with four short Mn—Er contacts of 3.398(1) Å and four long contacts of greater than 3.6 Å. The shorter distances are within the sum of covalent radii and are therefore consistent with weak bonds, but the longer ones are too long to be genuine bonding interactions. The capping Er atoms also bond to the main group elements of the octahedron, with bond lengths ranging between 2.866(6) and 3.030(1) Å. The next polyhedral layer completes the coordination sphere of the main group elements in the inner octahedron, and is also formed entirely by main group elements that are arranged in a distorted truncated octahedron. The octahedral character of this polyhedron arises from the Jahn—Teller distorted octahedron immediately surrounding Mn5, and the larger truncated octahedron retains the same D_{4h} symmetry seen in the inner distorted octahedron. These main group sites are all bonded directly to the distorted cube of Er atoms, which sit on the faces of the truncated octahedron. The outermost layer of the Mn5-centered cluster is a distorted rhombicuboctahedron composed entirely of Mn atoms, occupying three distinct crystallographic positions. These clusters, if viewed as individual units, are arranged in a face centered cubic arrangement (Figure 4).

Table 3. Selected Interatomic Distances in the $RE_5Mn_4Al_{23-x}Si_x$ System[a]

bond name	multiplicity	Ho	Er	Yb
RE(1)—Al/Si(4)	8	2.8586(13)	2.8458(17)	2.8561(17)
RE(2)—Al/Si(5)	4	2.8748(6)	2.8617(7)	2.8625(7)
RE(2)—Al/Si(2)	4	3.0495(11)	3.0364(14)	3.0269(13)
RE(2)—Al/Si(6)	1	3.0504(4)	3.0441(4)	3.0451(4)
Mn(1)—Al/Si(4)	2	2.4172(11)	2.4130(15)	2.3961(15)
Mn(1)—Al/Si(1)	2	2.5184(10)	2.5126(12)	2.5349(11)
Mn(1)—Al/Si(2)	4	2.5843(9)	2.5753(13)	2.5781(12)
Mn(1)—Al/Si(6)	1	2.3804(11)	2.3671(14)	2.3721(13)
Al/Si(3)—Al/Si(5)	4	2.664(2)	2.650(3)	2.665(2)

[a] All distances are given in angstroms.

Table 4. Atomic Positions for $Er_{44}Mn_{55}(AlSi)_{237}$

atom	x	y	z	Wyckoff label	U_{eq}
Er(1)	0	0.2204(1)	0.2912(1)	24*k*	6(1)
Er(2)	0	0.3626(1)	0.4081(1)	24*k*	8(1)
Er(3)	0	0.3705(1)	0.0865(1)	24*k*	8(1)
Er(4)	0.0915(1)	0.0915(1)	0.0915(1)	16*i*	7(1)
Mn(1)	0.0959(1)	0.1097(1)	0.2469(1)	48*l*	5(1)
Mn(2)	0	0.3629(2)	0.2541(2)	24*k*	8(1)
Mn(3)	1/4	0.6034(1)	0.1034(1)	24*j*	6(1)
Mn(4)	1/4	1/4	1/4	8*e*	5(1)
Mn(5)	0	1/2	1/2	6*b*	7(2)
Al/Si(1)	0.0632(2)	0.4344(2)	0.1916(2)	48*l*	9(1)
Al/Si(2)	0.0634(2)	0.1920(2)	0.1794(2)	48*l*	8(1)
Al/Si(3)	0.0725(2)	0.3072(2)	0.1890(2)	48*l*	12(1)
Al/Si(4)	0.0827(2)	0.3180(2)	0.3109(2)	48*l*	3(1)
Al/Si(5)	0.0884(2)	0.1381(2)	0.3619(2)	48*l*	11(1)
Al/Si(6)	0.1421(2)	0.2126(2)	0.2871(2)	48*l*	12(1)
Al/Si(7)	0	0.0793(2)	0.3015 (2)	24*k*	7(2)
Al/Si(8)	0	0.0847(2)	0.4222(2)	24*k*	6 (1)
Al/Si(9)	0	0.0960(3)	0.1901(2)	24*k*	7(1)
Al/Si(10)	0	0.2171(3)	0.4252(2)	24*k*	10(2)
Al/Si(11)	0	0.2216(3)	0.0798(3)	24*k*	13(2)
Al/Si(12)	1/4	0.1745(2)	0.6745(2)	24*j*	4(1)
Al/Si(13)	0.1779(2)	0.1779(2)	0.1779(2)	16*i*	15(2)
Al/Si(14)	0.1117(3)	0	1/2	12*g*	3(2)
Al/Si(15)	0.1255(3)	0	0	12*f*	5(2)
Al/Si(16)	0	0	0	2*a*	4(3)

Table 5. Selected Interatomic Distances for $Er_{44}Mn_{55}(AlSi)_{237}$

bond name	distance (Å)	bond name	distance (Å)
Er(1)−Al/Si(4)	2.825(4)	Mn(1)−Al/Si(7)	2.498(3)
Er(1)−Al/Si(2)	2.871(4)	Mn(1)−Al/Si(3)	2.551(5)
Er(1)−Al/Si(10)	2.926(5)	Mn(2)−Al/Si(4)	2.399(4)
Er(1)−Al/Si(5)	3.054(4)	Mn(2)−Al/Si(3)	2.450(5)
Er(2)−Al/Si(8)	2.868(4)	Mn(2)−Al/Si(1)	2.460(5)
Er(2)−Al/Si(4)	2.949(4)	Mn(3)−Al/Si(4)	2.429(4)
Er(2)−Al/Si(5)	3.014(4)	Mn(3)−Al/Si(10)	2.447(3)
Er(3)−Al/Si(8)	2.873(4)	Mn(3)−Al/Si(5)	2.578(4)
Er(3)−Al/Si(14)	2.8792(16)	Mn(4)−Al/Si(12)	2.330(5)
Er(3)−Al/Si(7)	2.972(4)	Mn(4)−Al/Si(6)	2.619(4)
Er(3)−Al/Si(1)	3.018(4)	Mn(5)−Al/Si(14)	2.438(7)
Er(4)−Al/Si(15)	2.920(2)	Mn(5)−Al/Si(8)	2.509(5)
Er(4)−Al/Si(9)	2.936(4)	Al/Si(1)−Al/Si(1)	2.548(7)
Mn(1)−Al/Si(2)	2.403(4)	Al/Si(1)−Al/Si(4)	2.620(5)
Mn(1)−Al/Si(2)	2.428(4)	Al/Si(1)−Al/Si(14)	2.643(6)
Mn(1)−Al/Si(9)	2.451(3)	Al/Si(1)−Al/Si(3)	2.786(6)
Mn(1)−Al/Si(11)	2.481(2)	Al(16)−Al(15)	2.739(7)

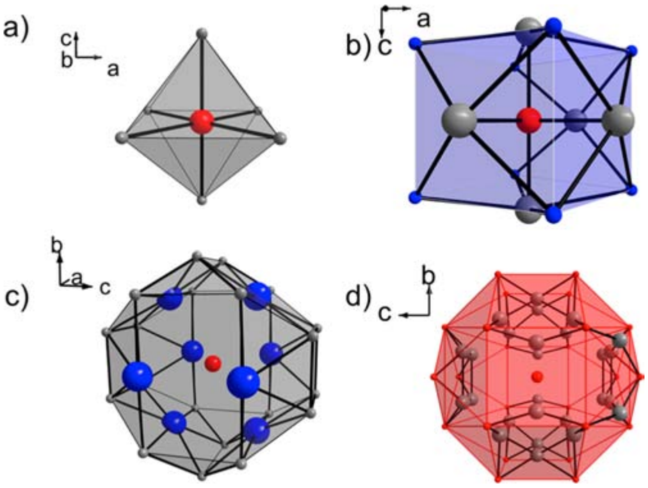

Figure 5. Nested polyhedra centered on the Mn5 position in $Er_{44}Mn_{55}(AlSi)_{237}$, consisting of (a) a distorted octahedron surrounded by (b) a distorted cube, whose vertexes lie on the faces of (c) a distorted truncated octahedron, which is surrounded by (d) an irregular rhombicuboctahedron. As in Figure 4, blue represents Er, red represents Mn, and gray represents mixed Al/Si sites.

The packing of Mn5-centered clusters leaves substantial voids in the structure, which are mostly filled by a second cluster of nested polyhedra centered on the main group atom X16, situated on Wyckoff position 2*a* and shown in Figure 6. The first coordination sphere of X16 consists of a perfect octahedron of main group atoms, with a bond length of 2.736(6) Å. As is the case in the Mn5-centered cluster, Er atoms cap the faces of the octahedron. However, in this case, the Er cube is not distorted and therefore composed of a single crystallographic Er site. The Er−X16 distance in this case is 3.459(1) Å, well beyond the sum of covalent radii and therefore too long to be a genuine bond. Er does bond to the atoms that form the octahedron, with bond lengths of 2.919(2) Å.

After the first two polyhedral layers, the X16 cluster structure becomes more complex. The next layer is best described as two independent polyhedra that are a nearly identical distance from the central X16 position. The first is a regular icosahedron, formed by X9 atoms, each of which directly bond to both the Er cube and the inner octahedron (Figure 6c). The Er atoms sit on faces of the icosahedron. The X9 atoms are also directly bonded to X11 atoms, which form a distorted icosahedron

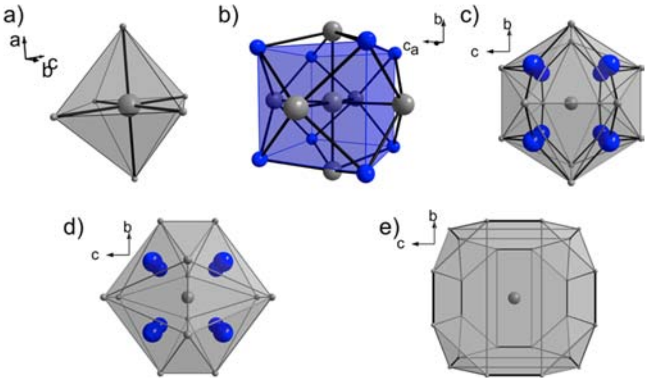

Figure 6. Set of regular nested polyhedra centered about the X16 main group position in $Er_{44}Mn_{55}(AlSi)_{237}$. The first coordination sphere consists of a regular octahedron, shown in (a). This is followed by a cube of Er atoms (b). Beyond this there is a choice of a regular (c) or distorted (d) icosahedron, both composed entirely of main group atoms. The outermost polyhedron of this set is a slightly distorted truncated cube also composed entirely of main group atoms, shown in (e). The stretched icosahedron shown in (d) protrudes slightly from the faces of the truncated cube shown in (e).

(Figure 6d) with a volume similar to that of the X9 regular icosahedron. The X11 atoms are also bonded directly to both the main group octahedron and the Er cube, and again the Er atoms sit on faces of the distorted icosahedron. Both icosahedra form some bonds to the adjacent Mn4 positions, which form the outer shell of the major polyhedral cluster centered on Mn5. The outermost layer of the X16-centered cluster is situated immediately outside these two interpenetrating icosahedra. It is a truncated cube composed of a single main group crystallographic position, X2 (Figure 6e). X2 bonds directly to Mn1, the outer shell of the Mn3-centered cluster. X2 also links to the Mn2 rhombicuboctahedron through bridging X3 atoms. If the two clusters are viewed as single units, they form an interpenetrating double network of the perovskite structure (Figure 4a).

These two clusters describe a majority of the structure, but leave significant gaps. The remaining atoms can nearly all be described as simple polyhedra that bridge the previously described clusters, or as more direct single-atom bridges. The most notable structure not described by the nested clusters is centered on the Mn4 position (Figure 7a), at Wyckoff position 8*e*. Mn4 is coordinated by a capped triangular prism of main group atoms very similar to the manganese coordination in the tetragonal $RE_5Mn_4Al_{23-x}Si_x$ compounds. The polyhedron around Mn4 differs, however, in that the prism is vertically compressed so that the central Mn atom actually bonds to two additional main group atoms, which cap the top and bottom faces of the prism. This capped triangular prism is directly bonded to the Mn rhombicuboctahedron and distorted truncated octahedron of main group atoms centered on the Mn5 position, as well as the truncated cube of main group positions centered on X16. The triangular prism also shares vertexes with an irregular, 10-vertex polyhedron centered on Er1 at Wyckoff position 24*k* (Figure 7b). The vertexes of this polyhedron are all main group positions, and nearly all of them participate in either the outer layers of the nested polyhedra or triangular prism. These two polyhedra, in addition to the nested polyhedra centered on Mn5 and X16, describe all of the atomic positions in the structure with the exception of a single main group position, X11, which sits near one of the faces of the Mn rhombicuboctahedron and bridges it directly to the main group truncated cube.

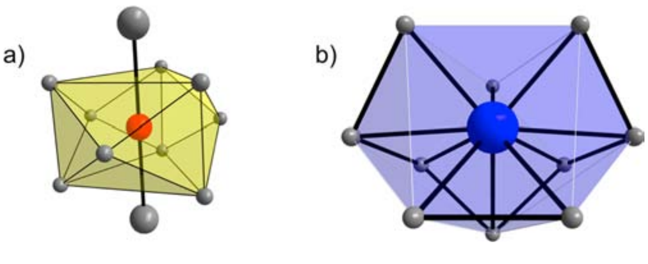

Figure 7. (a) Trigonal prism centered on Mn1 in $Er_{44}Mn_{55}(AlSi)_{237}$, capped on every face. The main group atoms, drawn independent of the polyhedron, bridge the Mn to the Er1 position. This coordination environment strongly resembles that of Mn in $RE_5Mn_4Al_{23-x}Si_x$. (b) Er1 position in $Er_{44}Mn_{55}(AlSi)_{237}$, coordinated by an irregular, 10-vertex polyhedron consisting entirely of main group atoms viewed approximately down the *b*-axis.

Viewing structures through the lens of nested polyhedra is a common method for understanding highly complex intermetallic structures. Despite this, meaningful structural relationships between $Er_{44}Mn_{55}(AlSi)_{237}$ and previously reported compounds are not immediately obvious. No exact analogues of the nested polyhedra described above have been reported in previous literature to our knowledge. However, a local structure fragment analogous to the inner cluster structure of a central atom centering an octahedron surrounded by a cube observed in the two major clusters of $Er_{44}Mn_{55}(AlSi)_{237}$ in both a distorted and an undistorted form is also seen in Al-rich Ti−Co−Al compounds known as G-phases, which have compositions near $Ti_{30}Co_{25}Al_{45}$ and adopt a variant of the Th_6Mn_{23} structure type.[40] Additionally, the packing of the major clusters in a perovskite arrangement (Figure 4) is topologically identical to cluster packing in $Li_6A_{17}Hg_9$,[41] although the clusters themselves are substantially different from those observed in $Er_{44}Mn_{55}(AlSi)_{237}$.

Electrical Resistivity. All of the reported compounds are metallic and exhibit the expected direct dependence between resistivity and temperature when measured along the *c* direction in the range of 2−300 K, shown in Figure 8. $Ho_5Mn_4Al_{23-x}Si_x$ is the only compound that shows evidence of a phase transition, with a distinct drop in resistivity at 13.4 K. This transition is second order and most likely is a result of magnetic ordering, discussed below.

Magnetic Properties. The magnetic behavior of three of the title compounds, $Er_5Mn_4Al_{23-x}Si_x$, $Yb_5Mn_4Al_{23-x}Si_x$, and $Er_{44}Mn_{55}(AlSi)_{237}$, can be fit to a modified Curie−Weiss model between 6 and 300 K. No magnetic deviations away from the paramagnetic state were observed for any of these compounds. Plots of magnetic susceptibility versus temperature are shown in Figure 9a−c, and the parameters for Curie−Weiss fits are shown in Table 6, along with resistivity information. All three compounds were fit to a modified Curie−Weiss law:

$$\chi = \chi_0 + \frac{C}{T - \Theta}$$

In this equation, χ_0 represents a temperature-independent term corresponding to Pauli paramagnetism, C is the Curie constant, and Θ is the Weiss constant. All three compounds exhibit a negative Weiss constant, indicating antiferromagnetism, but antiferromagnetic transitions were not observed in the measured range for any of the three compounds.

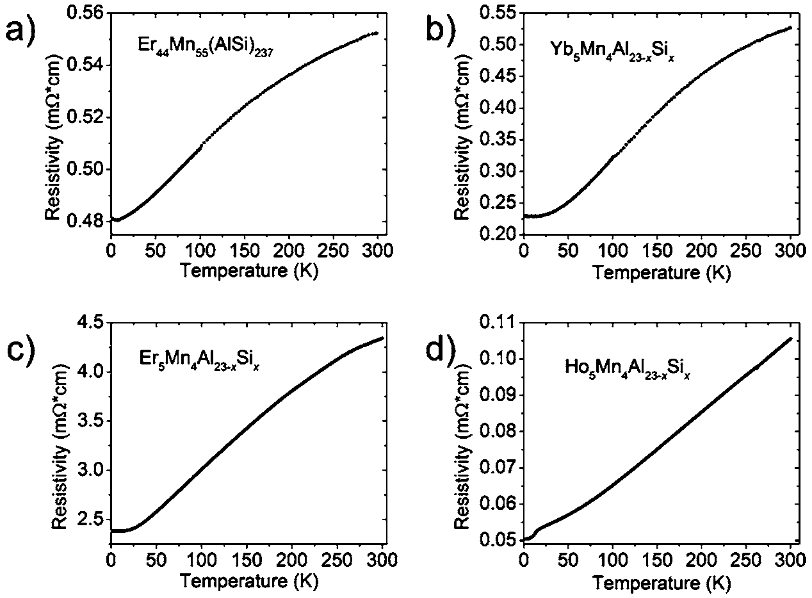

Figure 8. Temperature-dependent resistivity plots of $Er_{44}Mn_{55}(AlSi)_{237}$ and $RE_5Mn_4Al_{23-x}Si_x$ (RE = Yb, Er, and Ho) are shown in (a)−(d), respectively. All exhibit normal metallic conduction, with $Ho_5Mn_4Al_{23-x}Si_x$ showing a small drop in resistivity at 13 K, likely caused as a result of magnetic ordering. The plot in (d) also required a small correction for an instrumental artifact at ~263 K.

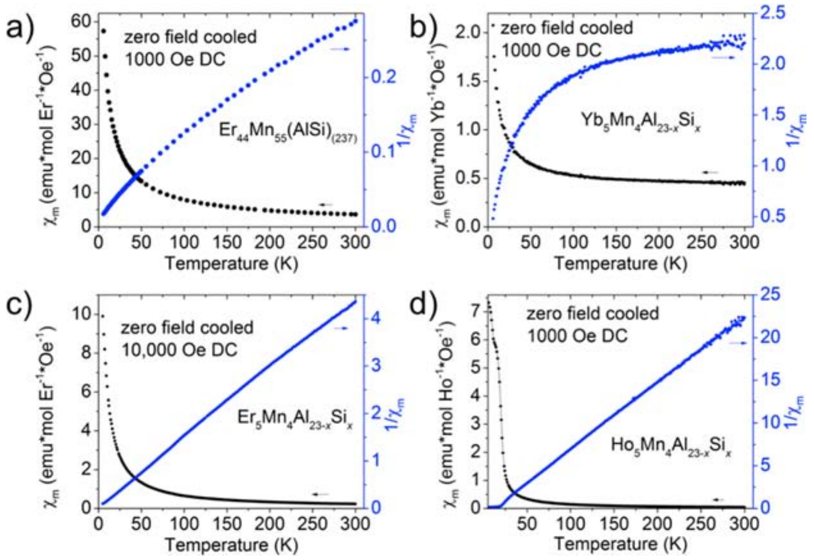

Figure 9. Plots of temperature-dependent magnetic susceptibility for $Er_{44}Mn_{55}(AlSi)_{237}$ and $RE_5Mn_4Al_{23-x}Si_x$ (RE = Yb, Er, and Ho), respectively. All four plots show only zero field cooled susceptibility and inverse susceptibility, which under these measurement conditions appear identical to the field cooled case. All of the compounds follow either the Curie−Weiss law either with a temperature-independent term to account for Pauli paramagnetism in the case of (a) and (b) or without it in the case of (c) and (d). $Ho_5Mn_4Al_{23-x}Si_x$ (d) exhibits two transitions below 25 K, shown in more detail in Figure 10.

Table 6. Fitted Parameters of the Modified Curie−Weiss Law Describing the Measured Magnetic Properties of the Four Title Compounds, Measured on Single Crystals[a]

compound	C (emu/mol·K)	Θ (K)	χ_0 (emu/mol)	moment per RE atom (μ_B)
$Ho_5Mn_4Al_{23-x}Si_x$	63.62(5)	12.79(8)	0	4.51(1)
$Er_5Mn_4Al_{23-x}Si_x$	358(2)S	−1.78(5)	0	10.7(8)
$Yb_5Mn_4Al_{23-x}Si_x$	58.8(4)	−1.31(7)	2.070(4)	4.3(3)
$Er_{44}Mn_{55}(AlSi)_{237}$	$2.75(2) \times 10^4$	−5.35(10)	81(2)	10.6(9)

[a] The fits used the equation discussed in the text and the data shown in Figure 10. Notice that the values in the first three columns are per formula unit, not per RE atom.

$Yb_5Mn_4Al_{23-x}Si_x$ (Figure 9a) has the largest temperature-independent contribution of 2.070(4) emu/formula unit, which originates from the Pauli paramagnetism exhibited by itinerant electrons. The Curie constant yields a total paramagnetic

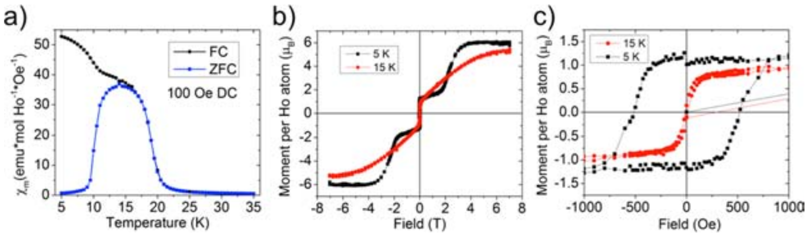

Figure 10. Low-field temperature-dependent magnetization (a) and field-dependent magnetization measurements (b,c) on $Ho_5Mn_4Al_{23-x}Si_x$. Two transitions are apparent in (a), one at 10 K and the other at 20 K. Hysteresis loops at 5 K (black) and at 15 K (red) seek to elucidate the nature of these transitions. Part (b) depicts the full scale of both measurements to 7 T, while (c) zooms in on the plot's origin. Note that (b) denotes field in T, while (c) denotes field in Oe. Both measurements suggest ferromagnetic order at the given temperatures. The 5 K measurement shows an initial saturation point at low field corresponding to the moment of a single Ho atom, with further magnetization at higher field. This feature is absent at 15 K, suggesting the presence of two distinct magnetic lattices that order at different temperatures. The noise at high field is likely a result of slight sample reorientation while the crystals attempt to adopt a more favorable alignment with the applied field.

moment of 4.3(3) μ_B per Yb atom, which is consistent with the theoretical value of ~4.5 μ_B for Yb^{3+}. Alternatively, this moment can be interpreted as a paramagnetic moment of 5.4(4) μ_B per Mn atom, which is comparable to the theoretical spin-only moment of 5.9 μ_B. This value suggests two competing interpretations: that the Mn present in the unit cell is magnetically silent and the only magnetic contributions are from Yb^{3+}, or that all of the Yb present are in the Yb^{2+} state, and only Mn moments contribute to the non-Pauli paramagnetic behavior. The cell parameters of the Yb analogue are more consistent with Yb^{3+} than with the substantially larger Yb^{2+} ion, suggesting that the first interpretation is the correct one. Furthermore, Mn bears no moment in both of the Er compounds, and we believe that in light of both this and the trends in unit cell parameters it is most likely that Mn is magnetically silent in $Yb_5Mn_4Al_{23-x}Si_x$.

Fits of $Er_5Mn_4Al_{23-x}Si_x$ (Figure 9b) with a nonzero Pauli contribution were unsuccessful, suggesting that the Pauli contribution is negligible as compared to the local moments. The moment per Er atom is 10.7(8) μ_B when calculated from the Curie constant. This value is slightly larger than the theoretical value for Er^{3+} of 9.6 μ_B, suggesting that there is perhaps some small magnetization arising from the Mn atoms. If distributed evenly among Mn atoms, this small magnetic moment would correspond to slightly more than 1 μ_B per Mn. The magnetic data from $Er_{44}Mn_{55}(AlSi)_{237}$ (Figure 9c) yield an essentially identical moment per Er atom of 10.6(9) μ_B, although the cubic compound does exhibit a small but measurable Pauli contribution. A magnetically silent transition metal is also seen in all reported rare earth iron aluminum silicides,[21,24] the only other observed first row transition metal compounds of this class that exhibit crystallographically unique, ordered transition metal sites, to our knowledge. Mn atoms that are magnetically silent or have small local moments have also been observed in the ternary $REMn_4Al_8$ system,[42] where RE stands for rare earth, and both moment-bearing as well as magnetically silent Mn atoms have been observed in the $REMn_6Al_6$[43] and $REMn_{2+x}Al_{10-x}$[44] systems.

The magnetic properties of $Ho_5Mn_4Al_{23-x}Si_x$ deviate substantially from those of the other three title compounds (Figure 9d). It exhibits two independent, second-order magnetic transitions at 20 and 10 K, as determined by peaks in $d\chi/dT$. The two transitions appear the same in both field cooled and zero field cooled experiments at 1000 Oe but differently at 100 Oe, suggesting some field-dependence of the transitions. The 20 K transition appears to be ferromagnetic in character, followed by an additional ordering transition that further increases magnetization. The compound obeys the Curie−Weiss law above these transitions, but as is the case in $Er_5Mn_4Al_{23-x}Si_x$, fitting with a nonzero Pauli paramagnetic term proved impossible. The Weiss constant is 12.79(8) K when fit above 75 K, further suggesting that at least one of the observed transitions signals the onset of ferromagnetic ordering. The overall calculated moment per Ho atom, however, is 4.51(1) μ_B, less than one-half the expected predicted value of 10.6 μ_B for free Ho^{3+}. Field-dependent magnetization experiments were carried out at both 5 and 15 K, below both apparent transitions observed in the temperature-dependent measurements and between the two, respectively (Figure 10). Measurements at both temperatures show magnetic hysteresis indicative of ferromagnetic ordering. The 5 K measurement exhibited step-like behavior, with an initial saturation of about 2 μ_B/Ho atom at around 1 T and increasing magnetization upon further increases in field, with an eventual saturation at around 4 T of 6 μ_B per Ho atom. This step feature is entirely absent in the 15 K measurement. As the structure exhibits two crystallographically distinct Ho sites, one accounting for one of the Ho atoms and the other accounting for four of them, and the theoretical moment of one Ho atom is 10.6 μ_B, this suggests independent ordering of two distinct Ho magnetic sublattices at 5 K but not at temperatures higher than the transition at 10 K. The 1 T step would, in this interpretation, correspond to ordering of one atom per unit cell, with further ordering occurring only at higher field. The measurement at 15 K shows a coercivity of 14 Oe and a remnant magnetization of 0.13 μ_B/Ho atom, while the measurements taken at 5 K show a substantially larger coercivity and remnant magnetization of 520 Oe and 1.1 μ_B/Ho atom. Both the reason for the unusually small moment derived from the Curie constant as well as the exact nature of the metamagnetic transition at 10 K remain unclear, and neutron diffraction experiments would be useful to further elucidate these points.

■ CONCLUSION

Four quaternary intermetallic compounds were prepared from Al flux: $RE_5Mn_4Al_{23-x}Si_x$ ($x = 7.9(9)$, RE = Ho, Er, Yb) and $Er_{44}Mn_{55}(AlSi)_{237}$. All crystallize in unusual or new structure types. The three $RE_5Mn_4Al_{23-x}Si_x$ compounds are the second series reported to crystallize in the $Gd_5Mg_5Fe_4Al_xSi_{18-x}$ structure type, and $Er_{44}Mn_{55}(AlSi)_{237}$ crystallizes in a complex new structure type, which is best described as a series of nested polyhedra. These intermetallic compounds exhibit normal metallic conductivity, and all but $Ho_5Mn_4Al_{23-x}Si_x$ demonstrate Curie−Weiss paramagnetism with antiferromagnetic order at low temperature. $Ho_5Mn_4Al_{23-x}Si_x$ exhibits more complex magnetic behavior, with ferromagnetic ordering as well as a second-order metamagnetic transition 10 K below the onset of ferromagnetic order. Neutron diffraction experiments are required to further understand the exact nature of this transition, as well as to confirm the assignments of Al and Si positions in the crystal structure.

■ ASSOCIATED CONTENT

Ⓢ Supporting Information

Combined crystallographic file in cif format for $RE_5Mn_4Al_{23-x}Si_x$ (RE = Ho, Er, Yb) and $Er_{44}Mn_{55}(AlSi)_{237}$. This material is available free of charge via the Internet at http://pubs.acs.org.

■ AUTHOR INFORMATION

Corresponding Author

*E-mail: m-kanatzidis@northwestern.edu.

Notes

The authors declare no competing financial interest.

■ ACKNOWLEDGMENTS

Research at Argonne is supported by the U.S. Department of Energy, Office of Science, Office of Basic Energy Sciences, Materials Sciences and Engineering Division (Argonne contract no. DE-AC02-06CH11357). We gratefully acknowledge the assistance of Prof. Danna Freedman and her research group, as well as support from Northwestern University's International Institute for Nanotechnology and the State of Illinois Department of Commerce and Economic Opportunity (DCEO) Award #10-203031, which facilitated some of the magnetic measurements. We also thank Dr. Lei Fang for some experimental help.

■ REFERENCES

(1) Andres, K.; Graebner, J. E.; Ott, H. R. *Phys. Rev. Lett.* **1975**, *35*, 1779.

(2) Steglich, F.; Aarts, J.; Bredl, C. D.; Lieke, W.; Meschede, D.; Franz, W.; Schäfer, H. *Phys. Rev. Lett.* **1979**, *43*, 1892.

(3) Kuga, K.; Morrison, G.; Treadwell, L.; Chan, J. Y.; Nakatsuji, S. *Phys. Rev. B* **2012**, *86*, 224413.

(4) Tobash, P. H.; Ronning, F.; Thompson, J. D.; Bobev, S.; Bauer, E. D. *J. Solid State Chem.* **2010**, *183*, 707.

(5) Cava, R. J.; Zandbergen, H. W.; Batlogg, B.; Eisaki, H.; Takagi, H.; Krajewski, J. J.; Peck, W. F.; Gyorgy, E. M.; Uchida, S. *Nature* **1994**, *372*, 245.

(6) Gofryk, K.; Ronning, F.; Zhu, J. X.; Ou, M. N.; Tobash, P. H.; Stoyko, S. S.; Lu, X.; Mar, A.; Park, T.; Bauer, E. D.; Thompson, J. D.; Fisk, Z. *Phys. Rev. Lett.* **2012**, *109*, 186402.

(7) Rotter, M.; Tegel, M.; Johrendt, D. *Phys. Rev. Lett.* **2008**, *101*, 107006.

(8) Fulfer, B. W.; Haldolaarachchige, N.; Young, D. P.; Chan, J. Y. *J. Solid State Chem.* **2012**, *194*, 143.

(9) Francisco, M. C.; Malliakas, C. D.; Macaluso, R. T.; Prestigiacomo, J.; Haldolaarachchige, N.; Adams, P. W.; Young, D. P.; Jia, Y.; Claus, H.; Gray, K. E.; Kanatzidis, M. G. *J. Am. Chem. Soc.* **2012**, *134*, 12998.

(10) Kangas, M. J.; Schmitt, D. C.; Sakai, A.; Nakatsuji, S.; Chan, J. Y. *J. Solid State Chem.* **2012**, *196*, 274.

(11) Löhneysen, H. v.; Pietrus, T.; Portisch, G.; Schlager, H. G.; Schröder, A.; Sieck, M.; Trappmann, T. *Phys. Rev. Lett.* **1994**, *72*, 3262.

(12) Jia, S.; Jiramongkolchai, P.; Suchomel, M. R.; Toby, B. H.; Checkelsky, J. G.; Ong, N. P.; Cava, R. J. *Nat. Phys.* **2011**, *7*, 207.

(13) Bauer, E. D.; Mixson, D.; Ronning, F.; Hur, N.; Movshovich, R.; Thompson, J. D.; Sarrao, J. L.; Hundley, M. F.; Tobash, P. H.; Bobev, S. *Physica B* **2006**, *378−380*, 142.

(14) Cable, J. W.; Koehler, W. C.; Wollan, E. O. *Phys. Rev.* **1964**, *136*, A240.

(15) Szytula, A.; Leciejewicz, J. *Handbook of Crystal Structures and Magnetic Properties of Rare Earth Intermetallics*; CRC Press: Boca Raton, FL, 1994.

(16) Ma, X.; Chen, B.; Latturner, S. E. *Inorg. Chem.* **2012**, *51*, 6089.

(17) Francisco, M. C.; Malliakas, C. D.; Piccoli, P. M. B.; Gutmann, M. J.; Schultz, A. J.; Kanatzidis, M. G. *J. Am. Chem. Soc.* **2010**, *132*, 8998.

(18) Chen, X. Z.; Sportouch, S.; Sieve, B.; Brazis, P.; Kannewurf, C. R.; Cowen, J. A.; Patschke, R.; Kanatzidis, M. G. *Chem. Mater.* **1998**, *10*, 3202.

(19) Sieve, B.; Chen, X.; Cowen, J.; Larson, P.; Mahanti, S. D.; Kanatzidis, M. G. *Chem. Mater.* **1999**, *11*, 2451.

(20) Sieve, B.; Chen, X. Z.; Henning, R.; Brazis, P.; Kannewurf, C. R.; Cowen, J. A.; Schultz, A. J.; Kanatzidis, M. G. *J. Am. Chem. Soc.* **2001**, *123*, 7040.

(21) Sieve, B.; Sportouch, S.; Chen, X. Z.; Cowen, J. A.; Brazis, P.; Kannewurf, C. R.; Papaefthymiou, V.; Kanatzidis, M. G. *Chem. Mater.* **2001**, *13*, 273.

(22) Latturner, S. E.; Bilc, D.; Mahanti, S. D.; Kanatzidis, M. G. *Chem. Mater.* **2002**, *14*, 1695.

(23) Latturner, S. E.; Bilc, D.; Mahanti, S. D.; Kanatzidis, M. G. *Inorg. Chem.* **2003**, *42*, 7959.

(24) Sieve, B.; Gray, D. L.; Henning, R.; Bakas, T.; Schultz, A. J.; Kanatzidis, M. G. *Chem. Mater.* **2008**, *20*, 6107.

(25) Canfield, P. C.; Fisk, Z. *Philos. Mag. B* **1992**, *65*, 117.

(26) Kanatzidis, M. G.; Pöttgen, R.; Jeitschko, W. *Angew. Chem., Int. Ed.* **2005**, *44*, 6996.

(27) Phelan, W. A.; Menard, M. C.; Kangas, M. J.; McCandless, G. T.; Drake, B. L.; Chan, J. Y. *Chem. Mater.* **2011**, *24*, 409.

(28) Latturner, S. E.; Kanatzidis, M. G. *Inorg. Chem.* **2008**, *47*, 2089.

(29) Latturner, S. E.; Kanatzidis, M. G. *Inorg. Chem.* **2003**, *43*, 2.

(30) Latturner, S. E.; Kanatzidis, M. G. *Inorg. Chem.* **2002**, *41*, 5479.

(31) Latturner, S. E.; Kanatzidis, M. G. *Chem. Commun.* **2003**, *0*, 2340.

(32) Shechtman, D.; Blech, I.; Gratias, D.; Cahn, J. W. *Phys. Rev. Lett.* **1984**, *53*, 1951.

(33) Elser, V.; Henley, C. L. *Phys. Rev. Lett.* **1985**, *55*, 2883.

(34) Biggs, B. D.; Pierce, F. S.; Poon, S. J. *Europhys. Lett.* **1992**, *19*, 415.

(35) Kranenberg, C.; Johrendt, D.; Mewis, A. *Z. Anorg. Allg. Chem.* **1999**, *625*, 1787.

(36) *X-Area Suite of Programs*; STOE & Cie GmbH: Darmstadt, Germany, 2006.

(37) Sheldrick, G. *Acta Crystallogr., Sect. A* **2008**, *64*, 112.

(38) Gelato, L. M.; Parthe, E. *J. Appl. Crystallogr.* **1987**, *20*, 139.

(39) Spek, A. *Acta Crystallogr., Sect. A* **1990**, *46*, c34.

(40) Grytsiv, A.; Rogl, P.; Giester, G.; Pomjakushin, V. *Intermetallics* **2005**, *13*, 497.

(41) Tkachuk, A. V.; Mar, A. *Chem.-Eur. J.* **2009**, *15*, 10348.

(42) Buschow, K. H. J.; Kraan, A. M. v. d. *J. Phys. F* **1978**, *8*, 921.

(43) Coldea, M.; Neumann, M.; Lütkehoff, S.; Mähl, S.; Coldea, R. *J. Alloys Compd.* **1998**, *278*, 72.

(44) Sefat, A. S.; Li, B.; Bud'ko, S. L.; Canfield, P. C. *Phys. Rev. B* **2007**, *76*, 174419.